Discovery and Optimization of Boronic Acid Based Inhibitors of Autotaxin

Harald M. H. G. Albers,[†,‡] Laurens A. van Meeteren,[†,⊥] David A. Egan,[∥,#] Erica W. van Tilburg,[†,∞]
Wouter H. Moolenaar,[†,§] and Huib Ovaa*[,†,‡]

[†]*Division of Cell Biology,* [‡]*Netherlands Proteomics Centre,* [§]*Centre for Biomedical Genetics,* and [∥]*Division of Molecular Carcinogenesis, The Netherlands Cancer Institute, 1066 CX Amsterdam, The Netherlands.* [⊥]*Current address: Department of Molecular Cell Biology, Leiden University Medical Center, Leiden, The Netherlands.* [#]*Current address: Department of Cell Biology, Utrecht University Medical Center, Utrecht, The Netherlands.* [∞]*Current address: Department of Nuclear Medicine, Erasmus Medical Center, Rotterdam, The Netherlands.*

Autotaxin (ATX) is an extracellular enzyme that hydrolyzes lysophosphatidylcholine (LPC) to produce the lipid mediator lysophosphatidic acid (LPA). The ATX−LPA signaling axis has been implicated in diverse physiological and pathological processes, including vascular development, inflammation, fibrotic disease, and tumor progression. Therefore, targeting ATX with small molecule inhibitors is an attractive therapeutic strategy. We recently reported that 2,4-thiazolidinediones inhibit ATX activity in the micromolar range. Interestingly, inhibitory potency was dramatically increased by introduction of a boronic acid moiety, designed to target the active site threonine in ATX. Here we report on the discovery and further optimization of boronic acid based ATX inhibitors. The most potent of these compounds inhibits ATX-mediated LPC hydrolysis in the nanomolar range ($IC_{50} = 6$ nM). The finding that ATX can be targeted by boronic acids may aid the development of ATX inhibitors for therapeutic use.

Introduction

Autotaxin (ATX[a] or NPP2), originally isolated as an autocrine motility factor from melanoma cells, belongs to the ecto-nucleotide pyrophosphatase and phosphodiesterase (NPP) family.[1−3] This extracellular enzyme acts as a lysophopholipase D, hydrolyzing lysophosphatidylcholine (LPC) into the lipid mediator lysophosphatidic acid (LPA), as depicted in Scheme 1.[4,5] Hydrolytic activity of ATX originates from a threonine (T210) residue in the active site.[1] LPA activates specific G-protein-coupled receptors and thereby stimulates the migration, proliferation, and survival of many cell types.[6]

The ATX−LPA axis has a vital role in vascular development.[7,8] Furthermore, it has been implicated in various pathologies including tumor progression[9] and metastasis,[10] inflammation,[11] and fibrotic disease.[12]

Given its role in human disease, the ATX−LPA axis is an obvious target for therapy. The fact that ATX is an extracellular enzyme makes it even more attractive as a drug target. Since there are at least six distinct LPA receptors, direct targeting of LPA receptors seems to be a less attractive strategy.[13,14] On the basis of the initial discovery that ATX is inhibited by LPA and sphingosine 1-phosphate (S1P) under

certain conditions,[15] various synthetic phospholipid analogues have been explored as ATX inhibitors.[16−20] However, lipid-based inhibitors have the disadvantage that they could act as agonists or antagonists for any of the LPA/S1P receptors, thereby resulting in an effect opposite of the one intended. In addition, non-lipid ATX inhibitors have been identified, but their inhibitory potential is low ($IC_{50} \geq 1\ \mu M$).[21−23]

Recently we reported the non-lipid ATX inhibitor HA130,[24] here named compound **72** (Table 3), that rapidly lowers plasma LPA levels upon intravenous injection in mice. Using inhibitor **72**, we found that the turnover of circulating LPA is much faster than expected, showing the usefulness of ATX inhibitors as tools to elucidate the role of ATX and LPA in vivo.

Here we describe the discovery and further optimization of compound **72**. We screened ∼40000 small molecules and identified thiazolidinediones as ATX inhibitors, which proved to be suitable to further chemical optimization. In particular, we optimized these molecules by first introducing small systematic variations in the structure of a screening hit, followed by the introduction of more random variations. Finally, by targeting the T210 oxygen nucleophile in ATX through a boronic acid, the potency of the original thiazolidinedione screening hit was increased over 400-fold ($IC_{50} = 6$ nM).

Results

ATX Inhibitor Screen. To identify ATX inhibitors, a small molecule screen was carried out. We first used a collection of 17 500 molecules from the National Cancer Institute (NCI) to optimize our screening protocol. This NCI library was initially screened using CPF4, an ATX activity reporter based on Förster resonance energy transfer (FRET) (Figure 1A).[15,25] The phosphodiester bond which links the coumarin and fluorescein moieties in CPF4 is hydrolyzed by

---

*To whom correspondence should be addressed. Address: Division of Cell Biology, The Netherlands Cancer Institute, Plesmanlaan 121, 1066 CX Amsterdam, The Netherlands. Phone: +31-20-5121979. Fax: +31-20-5122029. E-mail: h.ovaa@nki.nl.

[a]Abbreviations: ABTS, 2,2′-azino-bis(3-ethylbenzothiazoline-6-sulfonic acid); ATX, autotaxin; bis-pNPP, bis-*p*-nitrophenyl phosphate; HRP, horseradish peroxidase; HTS, high-throughput screening; FRET, Förster resonance energy transfer; LC−MS, liquid chromatography−mass spectrometry; LPA, lysophosphatidic acid; LPC, lysophosphatidylcholine; NCI, National Cancer Institute; NPP, nucleotide pyrophosphatase and phosphodiesterase; lysoPLD, lysophospholipase D; PI, percentage inhibition; RA, residual activity; SAR, structure−activity relationship; S1P, sphingosine 1-phosphate.

Scheme 1. Hydrolysis of LPC by ATX into LPA and Choline[a]
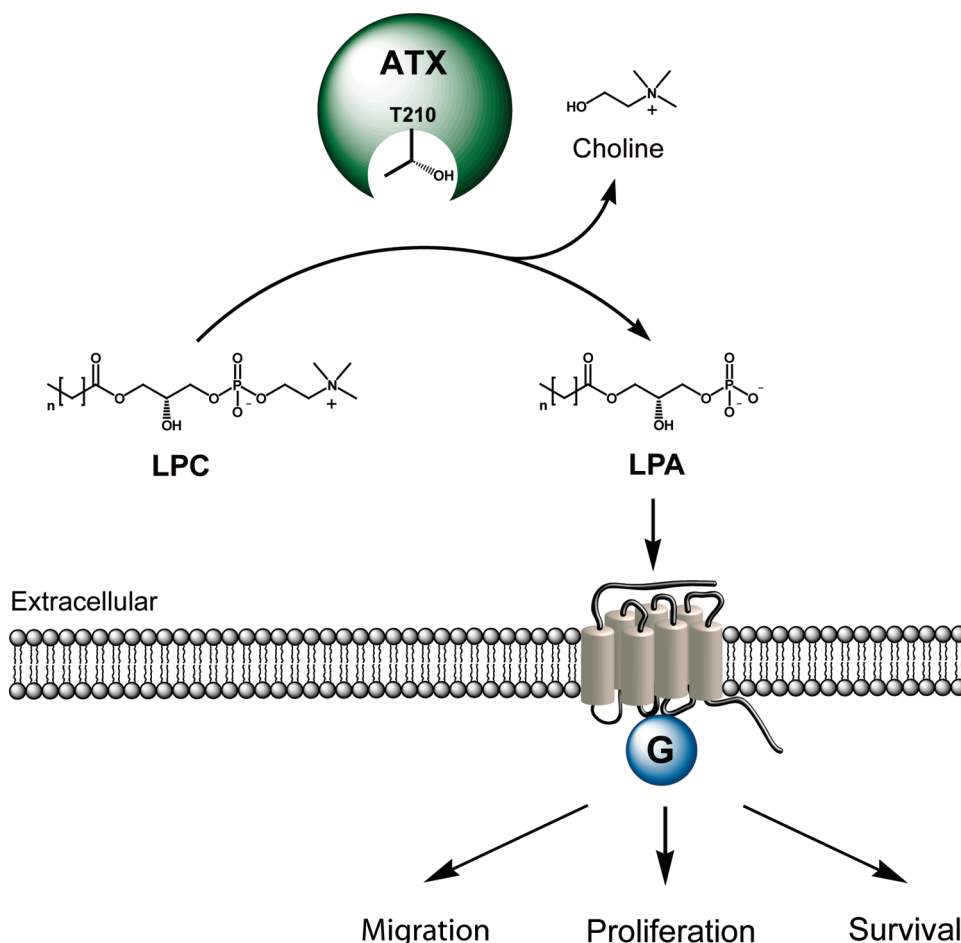
[a] The lysoPLD reaction is catalyzed by a threonine oxygen nucleophile (T210). Newly produced LPA triggers subsequent biological events via activation of specific G-protein-coupled receptors.

ATX, resulting in the loss of FRET. Since we have shown that LPA can inhibit ATX activity in this assay, it was used as a positive control for ATX inhibition.[15] Approximately 250 active molecules were retested in a second assay using bis-*p*-nitrophenyl phosphate (bis-pNPP) as reporter substrate (Figure 1B).[15] In Supporting Information Figure S1 the results of both assays are compared. Only a few compounds remained after retesting in the bis-pNPP assay. Since the CPF4 assay resulted in many false positives, we decided to reverse the assay order. The NCI library was tested in the bis-pNPP assay using CPF4 as confirmation tool which led to reproducible hits corresponding to the findings of Saunders et al.[26] Top three actives of the NCI screen can be found in Supporting Information Figure S2.

After validation of our screening protocol, we used a commercial library (SPECS) consisting of 23 000 small molecules with predicted druglike properties. For active molecules in this screen the percentage inhibition (PI) at $5\,\mu$M and IC$_{50}$ values (bis-pNPP assay) are shown in Figure 2. These actives were confirmed by the CPF4 assay (Figure 2). Among the confirmed active molecules were several 2,4-thiazolidinediones (**1**, **2**, **4**, and **5**), a pyrano pyrazole (**3**), and a benzothiazole (**6**). Because the 2,4-thiazolidinediones are well represented among the positive hits and because of their amenability to fast chemical diversification, the most potent 2,4-thiazolidinedione **2** (IC$_{50}$ = 56 nM) was selected for further optimization.

Chemistry. We next explored how to improve the potency of 2,4-thiazolidinedione **2** as an ATX inhibitor. We designed the convergent synthetic route toward inhibitor **2** depicted in Scheme 2. The synthesis requires benzoic acid **7** which can be obtained via a one-pot-synthesis. First, vanillin is O-alkylated with methyl 4-(bromomethyl)benzoate.[27] The resulting benzoate is hydrolyzed to give benzoic acid **7**. To afford the precursor **8**, 2,4-thiazolidinedione was dissolved in DMF and N-alkylated with 4-fluorobenzyl chloride in the presence of sodium hydride. Finally, monosubstituted thiazolane-2,4-dione **8** was reacted via a Knoevenagel condensation with benzoic acid **7**.[28] Z-Isomer **2** precipitated during reaction, and washing the precipitate with ethanol resulted in a homogeneous product.

The synthetic route toward **2** appeared to be applicable for the fast parallel synthesis and purification of many analogues without the need for chromatography.

Systematic Optimization. Inhibitor **2** contains two side chains attached to the thiazolidinedione core, a benzyl and a benzylidene moiety (Scheme 2). To explore structure–activity relationship (SAR), we first generated a small library before embarking on a bigger effort. This resulted in the molecules listed in Table 1. LPA was used as a control because it inhibits the ATX-mediated hydrolysis of bis-pNPP by ATX (IC$_{50}$ = 422 nM).[15]

The best series of inhibitors are the benzoic acids (**2** and **9**−**11**), where the fluorinated compound **2** has the highest
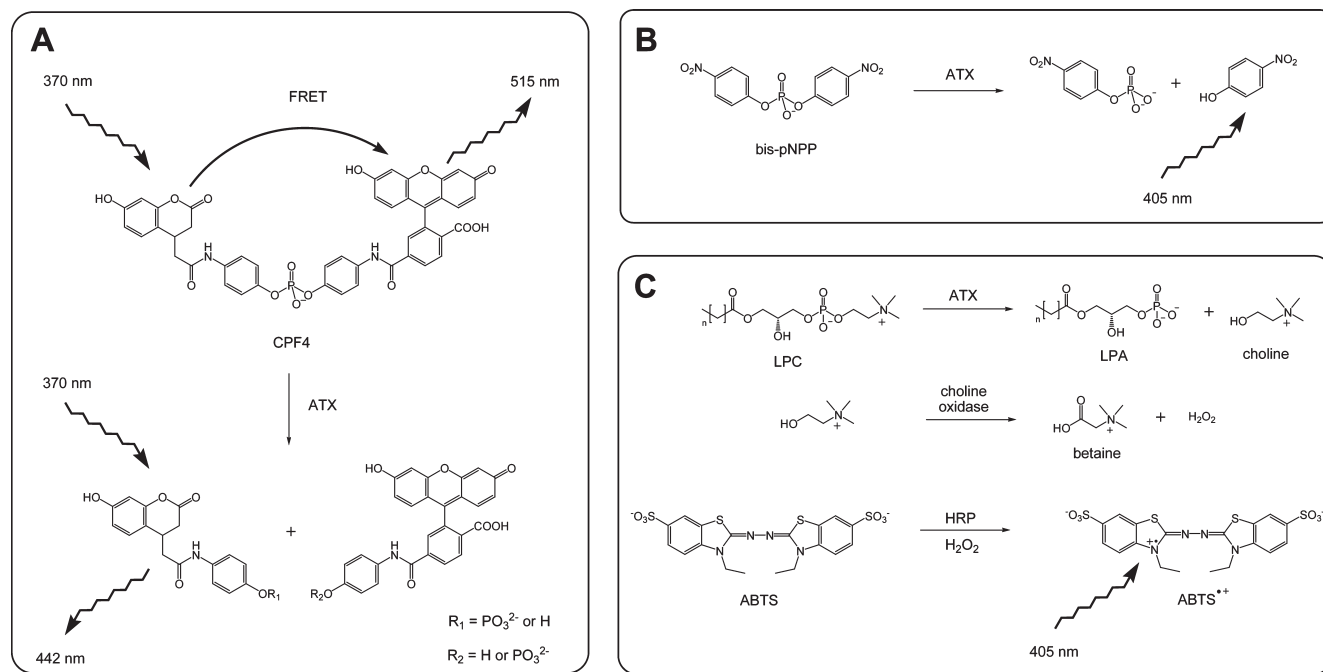
Figure 1. Three ATX assays used for screening and validation of ATX inhibitors. (A) CPF4 assay. This assay is based on Förster resonance energy transfer (FRET) between coumarin and fluorescein moieties of CPF4. (B) Bis-pNPP assay. In this assay bis-*p*-nitrophenyl phosphate (bis-pNPP) is hydrolyzed by ATX into the chromophore *p*-nitrophenol. (C) Choline release assay. The physiological substrate of ATX, LPC, is hydrolyzed by ATX to give LPA and choline. The release of choline can be detected in a two-step enzymatic coloring reaction.

activity (IC_{50} = 56 nM) in the bis-pNPP assay (Table 1). Replacement of the 4-fluorine atom (**2**) for hydrogen (**9**), 4-nitro- (**10**), or a *tert*-butyl group (**11**) reduced the potency of the inhibitor with increasing size of the functional group.

With replacement of the carboxylic acid in molecules **2** and **9**−**11** by a methyl ester (**12**−**15**), potency is largely lost. Omitting the carboxylic acid (**16**−**19**) has the same effect. With removal of the methoxy group (R2) in molecules **16**−**19**, activity is regained (compare **16**−**19** with **20**−**23**). SAR analysis showed that the optimal combination of groups would be R1 = −OCH₂−Ph−COOH, R2 = H, and R3 = F.

Encouraged by the SAR results suggesting that the methoxy and carboxylic acid groups are important moieties, molecules **28**−**30** were synthesized (Figure 3A). Molecules **2**, **9**−**11**, and **28**−**30** were validated in the physiologically more relevant LPC hydrolysis (choline release) assay.[17] The ATX-mediated release of choline from LPC is detected by a two-step enzymatic colorimetric reaction (Figure 1C). In the first step choline is oxidized by choline oxidase into betaine and hydrogenperoxide. Horseradish peroxidase (HRP) then consumes hydrogen peroxide to oxidize 2,2′-azino-bis(3-ethylbenzothiazoline-6-sulfonic acid) (ABTS) to a radical cation species which absorbs at 405 nm.

The data obtained from the choline release assay are summarized in Figure 3A. The IC_{50} values obtained were some 10-fold higher than observed in with bis-pNPP as a substrate. It is noteworthy that compound **10** is incapable of fully inhibiting ATX at high concentrations (Figure 3B). This residual ATX activity for **10** is about 60%. However, **10** shows inhibition at a lower concentration than **11** which was also observed in the bis-pNPP assay. LPA did not inhibit ATX in the choline release assay as observed by Ferry et al.[19]

The established SAR was confirmed by the more active molecule **28** (IC_{50} = 1.63 μM) in which the methoxy group in **2** (IC_{50} = 2.50 μM) is omitted. Changing the carboxylic acid

of **2** from para to the meta position results in the more potent inhibitor **29** (IC_{50} = 2.05 μM) but less potent than **28**. Changing the carboxylic acid in **28** from para to meta (**30**, IC_{50} = 1.07 μM) results in the most active molecule in this systematic optimization with a 2.5-fold reduction in IC_{50} value compared to **2** and also to a further reduction in residual ATX activity (from 35% to 7%) in the choline release assay.

Variation in the Benzyl Moiety. Since our initial systematic optimization of **2** provided good structure−activity correlations, we varied either the benzyl or the benzylidene moiety (Scheme 2). In this approach, either the benzyl or the benzylidene moiety corresponds to the screening hit **2** while the other part is alternated. First, the effect of changes in the benzyl part of the molecule was investigated by introducing halogens. The percentage inhibition (PI) values at 5 μM **31**−**40**, as measured by the choline release assay, are listed in Table 2. The most potent inhibitor was bromo compound **39** (PI = 73%). However, its IC_{50} (2.80 μM) is similar to that of screening hit **2** (IC_{50} = 2.50 μM). Other substituents that were explored did not result in significant improvements.

Variation in the Benzylidene Moiety. Next, variations were incorporated into the benzylidene moiety, resulting in molecules shown in Supporting Information Table S1. In contrast to the variation in the benzyl moiety, few molecules were active; only 30% of the compounds tested showed inhibition (PI_{max} = 5%). This indicates that variations in the benzylidene moiety of screening hit **2** are not well tolerated.

Boronic Acid Introduction and Optimization. Because the benzyl and benzylidene moiety variations did not improve inhibition, we modified inhibitor **30** that resulted from the systematic optimization. Replacing the carboxylic acid in molecule **30** by a boronic acid resulted in molecule **72** (Table 3). We recently characterized **72** as a potent ATX inhibitor both in vitro and in vivo.[24] We reasoned that the carboxylic acid moiety in molecule **30** could act as a phosphate
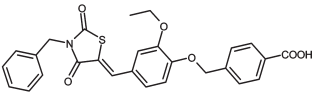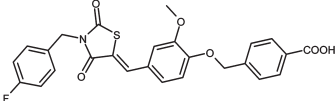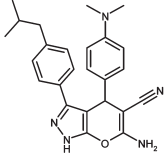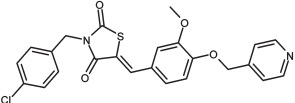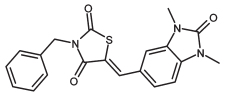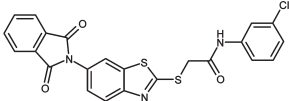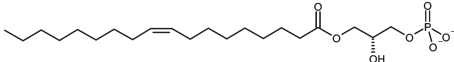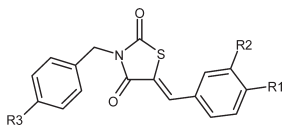
Structure	Nr.	PI (%)		IC$_{50}$ (nM)
		Bis-pNPP	*CPF4*	*Bis-pNPP*
	1	92	89	161
	2	91	85	56
	3	87	77	46
	4	83	85	68
	5	75	55	111
	6	71	66	261
	LPA	80	67	442

Figure 2. Molecules active as ATX inhibitors discovered by high-throughput screening. Percentage inhibition (PI) at 5 μM is based on the bis-pNPP or CPF4 assay. IC$_{50}$ values are obtained using the bis-pNPP assay. LPA was used as a control for ATX inhibition.

Scheme 2. Convergent Synthetic Route toward 2,4-Thiazolidinedione **2**^{a}
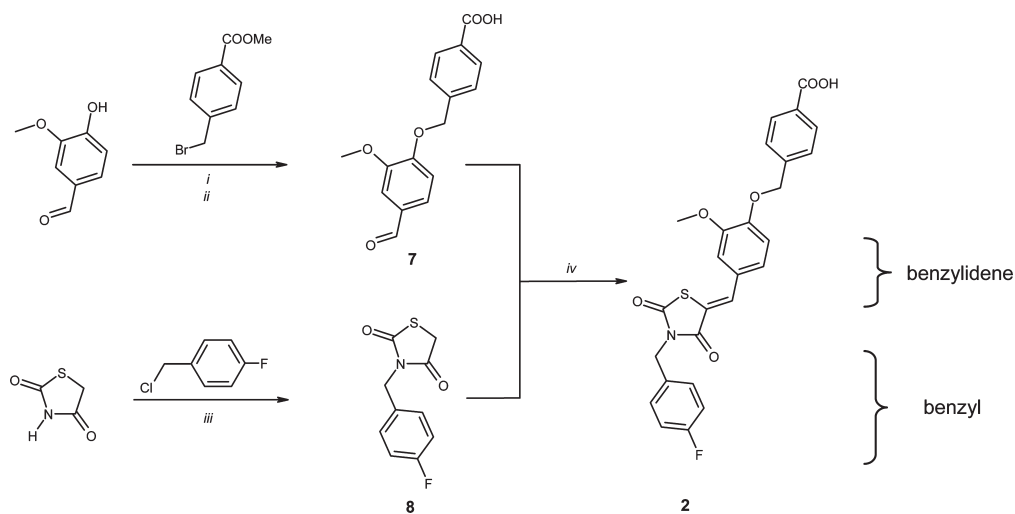
^{a} Reagents and conditions: (i) KOH, DMSO, room temp, 30 min; (ii) NaOH, DMSO/H$_2$O (1:3, v/v), reflux, 4 h, 91%; (iii) NaH, DMF, room temp, 22 h, 74%; (iv) piperidine, EtOH, reflux, 20 h, 63%.

Table 1. Structure−Activity Data for Molecules of the Systematic Optimization[a]

R1	R2	R3	Nr.	IC$_{50}$ (μM)	RA (%)
HOOC—⬡—CH$_2$—O---	OMe	H	9	0.248	9
	OMe	F	2	0.056	10
	OMe	NO$_2$	10	0.442	33
	OMe	C(CH$_3$)$_3$	11	18.2	33
MeOOC—⬡—CH$_2$—O---	OMe	H	12	2.69	24
	OMe	F	13	>100	-
	OMe	NO$_2$	14	60.9	31
	OMe	C(CH$_3$)$_3$	15	>100	-
⬡—O---	OMe	H	16	>100	-
	OMe	F	17	5.87	12
	OMe	NO$_2$	18	>100	-
	OMe	C(CH$_3$)$_3$	19	na	-
⬡—O---	H	H	20	2.69	32
	H	F	21	0.700	37
	H	NO$_2$	22	>100	-
	H	C(CH$_3$)$_3$	23	>100	-
H	H	H	24	>100	-
	H	F	25	>100	-
	H	NO$_2$	26	na	-
	H	C(CH$_3$)$_3$	27	na	-
LPA	-	-	LPA	0.442	39

[a] IC$_{50}$ Values and Residual ATX Activity (RA) of the Synthesized 2,4-Thiazolidinedione Derivatives Using the Artificial ATX Substrate bis-pNPP (na: not active at 5 μM).

A

R1	R2	R3	Nr.	IC$_{50}$ (μM)	RA (%)
HOOC—⬡—CH$_2$—O---	OMe	H	9	2.90	29
	OMe	F	2	2.50	35
	OMe	NO$_2$	10	>5	56
	OMe	C(CH$_3$)$_3$	11	13.6	27
	H	F	28	1.63	40
HOOC—⬡—CH$_2$—O---	OMe	F	29	2.05	42
	H	F	30	1.07	7

B

Figure 3. Validation of screening hit **2** and the benzoic acids of the systematic optimization in the choline release assay. (A) Structure−activity data of the systematic optimization. Residual ATX activity is abbreviated as RA (%). (B) Dose response curves for the benzoic acids.

mimic that binds near or at the active site threonine (T210). Replacing the carboxylic acid in molecule **30** by a boronic acid could well be a good ATX targeting strategy. This strategy was inspired by the proteasome inhibitor bortezomib, which targets the N-terminal threonine oxygen nucleophile in the proteasome through a boronic acid.[29] Furthermore, boronic acids have been reported to inhibit β-lactamases through targeting of the active site serine residue.[30]

The boronic acid modification resulted in a 100-fold more potent inhibitor (IC$_{50}$ = 28 nM) compared to screening hit **2** (IC$_{50}$ = 2.50 μM). When the position of the boronic acid was changed from meta (**72**) to the para (**73**) position, potency increased by another 5-fold (IC$_{50}$ = 5.7 nM) while the potency of the ortho boronic acid **74** dropped (IC$_{50}$ > 5.00 μM). Next, the 3-benzyloxyboronic acids analogues **75**−**77** were synthesized. The meta boronic acid (**75**) proved to be more potent than the para (**76**), and the ortho boronic acid (**77**) has a low potency.

Effect of Inhibitors on Readout Choline Release Assay. An inherent danger of the choline release assay is that small molecules can interfere with the readout by inhibiting the enzymes (horseradish peroxidase or choline oxidase) used in the coloring reaction, resulting in false positives. Another way to interfere with the choline release assay is that compounds can react with the ABTS or hydrogen peroxide generated during the coloring reaction. The latter could be an issue for the boronic acids reported here because aliphatic
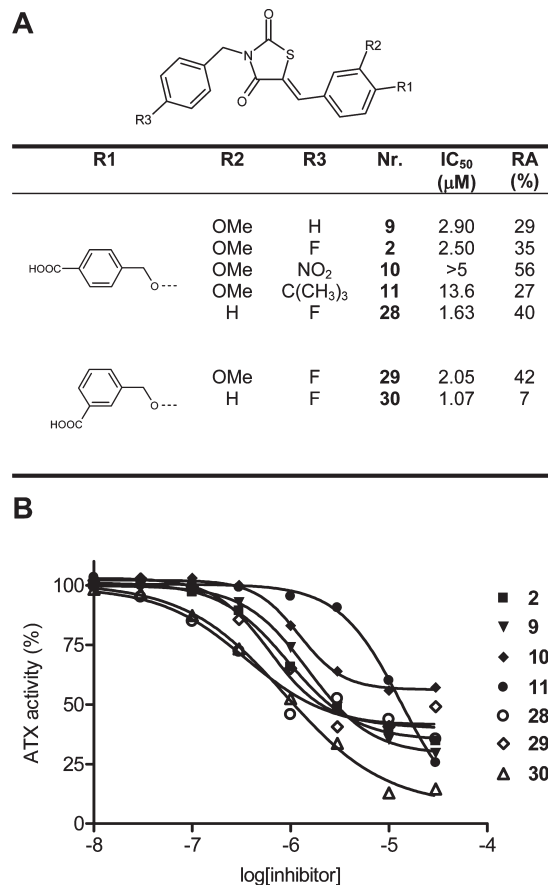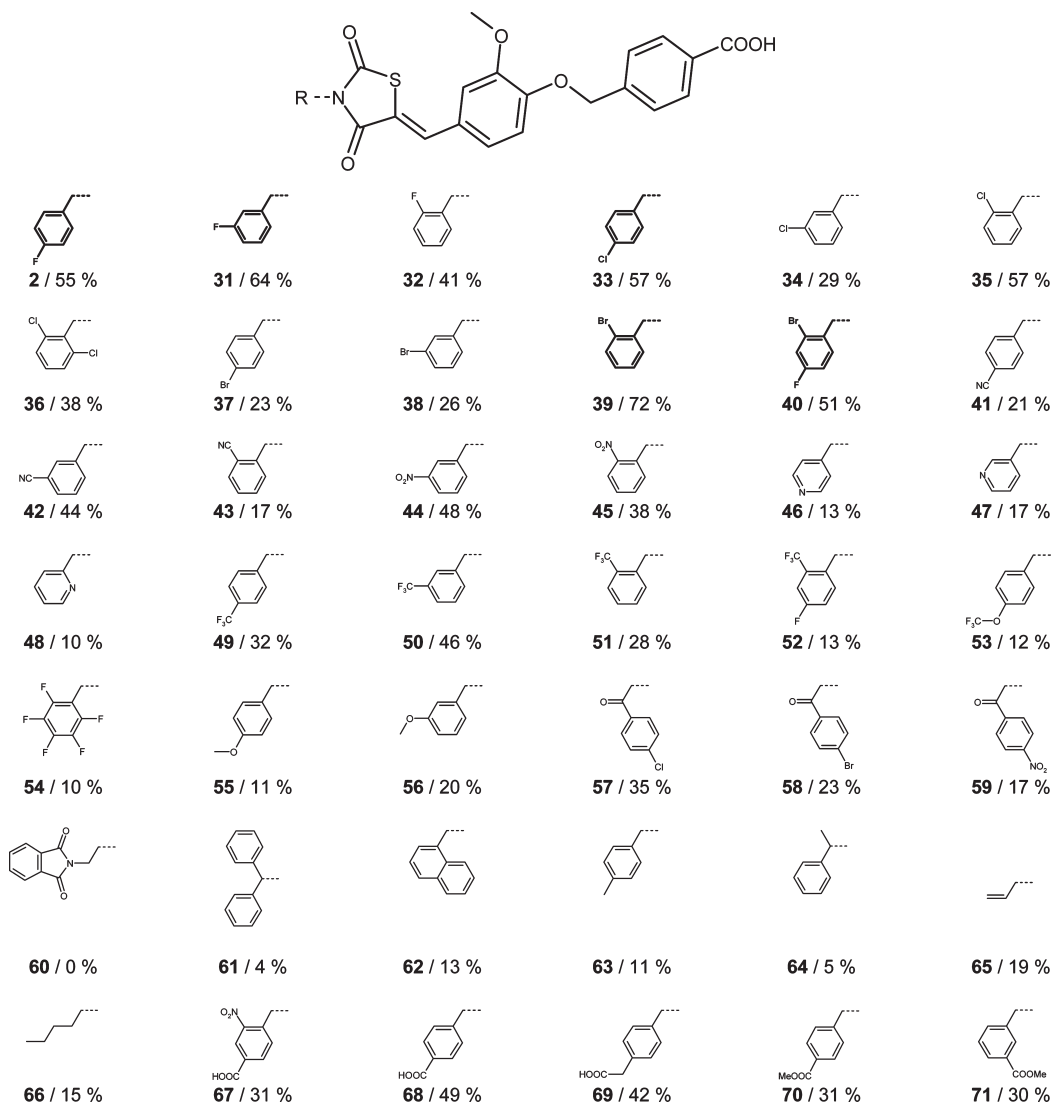
and aryl boronic acids have the intrinsic ability to react with hydrogen peroxide.[31−33] We investigated the effect of the inhibitors **72**, **73**, **75**, and **76** on the coloring reaction, and no effect was observed (Supporting Information Figure S3). Therefore, the choline release assay is a valid way to test the synthesized compounds here on ATX inhibition.

Mode of Inhibition. For inhibitors **2**, **30**, **72**, and **73**, the mode of inhibition was determined from a Lineweaver−Burk plot (Supporting Information Figure S4). Inhibitors **2** and **30** inhibit in a competitive manner using LPC as substrate. Kinetic analysis for boronic acids **72** and **73** revealed a mixed type inhibition.
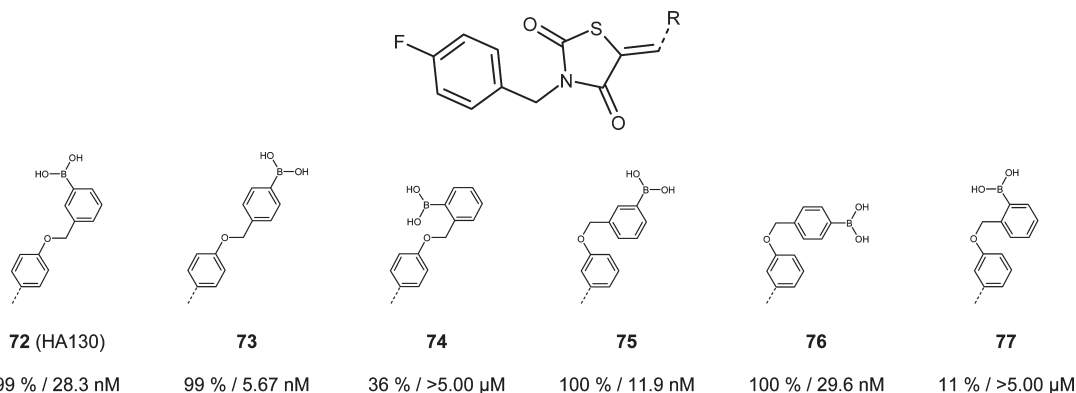
Because these inhibitors contain a Michael acceptor, it could be that these inhibitors react irreversibly with ATX (or other enzymes), which is undesirable. When ATX is incubated with 5 μM inhibitor **2**, **30**, **72**, or **73** for 20 min at 37 °C and these solutions are then washed with ethyl acetate, ATX activity is restored up to 97% of its original activity in the choline release assay (Supporting Information Figure S5). This indicates that these inhibitors reversible bind to ATX.

Discussion and Conclusions

This study shows that ATX can be targeted efficiently by boronic acids. We discovered thiazolidinediones as potent non-lipid ATX inhibitors. Replacing the carboxylic acid by a boronic acid in thiazolidinedione screening hit **2** resulted in a 440-fold more active inhibitor (IC$_{50}$ = 2.50 μM → 6 nM).

Table 2. Derivatives of Screening Hit **2** with a Structural Variation in the Benzyl Moiety[a]

2 / 55 %	**31** / 64 %	**32** / 41 %	**33** / 57 %	**34** / 29 %	**35** / 57 %
36 / 38 %	**37** / 23 %	**38** / 26 %	**39** / 72 %	**40** / 51 %	**41** / 21 %
42 / 44 %	**43** / 17 %	**44** / 48 %	**45** / 38 %	**46** / 13 %	**47** / 17 %
48 / 10 %	**49** / 32 %	**50** / 46 %	**51** / 28 %	**52** / 13 %	**53** / 12 %
54 / 10 %	**55** / 11 %	**56** / 20 %	**57** / 35 %	**58** / 23 %	**59** / 17 %
60 / 0 %	**61** / 4 %	**62** / 13 %	**63** / 11 %	**64** / 5 %	**65** / 19 %
66 / 15 %	**67** / 31 %	**68** / 49 %	**69** / 42 %	**70** / 31 %	**71** / 30 %

[a] Percentage inhibition (PI, %) has been determined in the choline release assay at 5 μM. Molecules that show more than 50% inhibition are in bold (**compound**/PI).

Table 3. Potent ATX Inhibitors of the Boronic Acid Optimization[a]

72 (HA130)	**73**	**74**	**75**	**76**	**77**
99 % / 28.3 nM	99 % / 5.67 nM	36 % / >5.00 μM	100 % / 11.9 nM	100 % / 29.6 nM	11 % / >5.00 μM

[a] For the boronic acids percentage inhibition (PI, %) at 5 μM and IC$_{50}$ values have been determined in the choline release assay (PI/IC$_{50}$).

We handed three different approaches for optimization of screening hit **2**. The first is the systematic optimization of **2**, which led to a 2.5-fold increase in potency in the choline release assay. The second is a randomized approach, changing separately the benzyl and the benzylidene parts of the molecule.

This did not result in significantly more potent molecules. Finally, we replaced the carboxylic acid in screening hit **2** by a boronic acid. Our rationale was that the carboxylic acid could function as a phosphate mimic and thereby bind near or at the T210 oxygen nucleophile. In that case, the T210 oxygen
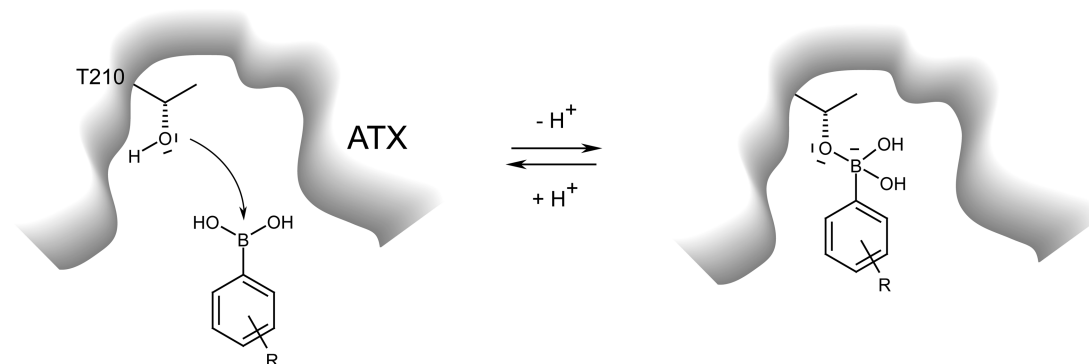
Figure 4. Our hypothesis on the binding of boronic acid **72** or **73** with the T210 oxygen nucleophile in the ATX active site.

nucleophile in ATX can be targeted via a boronic acid. A similar strategy has proven successful for the proteasome inhibitor bortezomib which binds to threonine oxygen nucleophile in the proteasome active site through the boronic acid moiety.[29] Replacing the carboxylic acid moiety in screening hit **2** (IC$_{50}$ = 2.50 μM) by a boronic acid resulted in molecule **73** (IC$_{50}$ = 6 nM), which is over 400-fold more potent than inhibitor **2**. These results demonstrate that ATX activity can be targeted by boronic acids.

Next to their increased affinity for ATX, the boronic acids are also expected to improve selectivity over hydrolytic enzymes that depend on a sulfur (cysteine) nucleophile, as is commonly found in phosphate ester hydrolyzing enzymes.

Kinetic analysis showed that inhibitors **2** and **30** inhibit in a competitive manner indicating that they bind at the active site of ATX. The acid moiety of these inhibitors likely mimics the phosphate group, facilitating inhibition. Boronic acids **72** and **73** show a mixed-type inhibition. It is expected that the boronic acids have the same binding site as their carboxylic acid equivalents **2** and **30** based on their structural similarity. Binding of the boronic acid to the T210 oxygen nucleophile likely results in the Lineweaver−Burk plot observed. The washout experiment reveals that inhibitors **2**, **30**, **72**, and **73** all bind to ATX in a reversible manner. Figure 4 shows how the boronic acid inhibitors may bind to the T210 oxygen nucleophile of ATX.

In summary, we have identified 2,4-thiazolidinediones as ATX inhibitors and have found that targeting ATX with a boronic acid moiety resulted in a > 400-fold increase in potency. This strategy to target ATX with a boronic acid should assist the development of future ATX inhibitors.

Experimental Section

Chemicals and Enzymes. Small molecule libraries were obtained from the National Cancer Institute (NCI) and purchased from SPECS, Delft, The Netherlands. NCI compounds NSC-101794, NSC148368, and NSC48300 are abbreviated in the text as **A**, **B**, and **C** respectively. SPECS compounds AN-989/40746701, AN-988/40680277, AJ-292/40674401, AN-989/41697652, AN-989/41697944, and AQ-088/4201464 are abbreviated in the text as **1**, **2**, **3**, **4**, **5**, and **6**, respectively. 1-Oleoyl-2-hydroxy-*sn*-glycero-3-phosphocholine (LPC, 18:1) was purchased from Avanti Polar Lipids. Oleoyl-L-α-lysophosphatidic acid sodium salt (LPA, 18:1), horseradish peroxidase (HRP), choline oxidase, and all other chemicals were obtained from Sigma-Aldrich and used as received. TALON-affinity beads were from Clontech, and opaque flat-bottom 96-well plates were from Greiner.

Recombinant ATX. HEK293 cells were transfected with the pcDNA3 vector containing a 6xHis-tagged human teratocarcinoma ATX sequence. After transfection, cells were washed and serum-free medium was added and cells were allowed to secrete His-tagged ATX into the culture medium for 48 h. Medium was collected and ATX was purified using TALON-affinity beads (Clontech) as described. Imidazole was removed by dialysis against Tris-buffered saline (140 mM NaCl, 5 mM KCl, 1 mM CaCl$_2$, 1 mM MgCl$_2$, and 50 mM Trizma, pH 8.0). Purity was verified by SDS−PAGE and Coomassie blue staining.

Bis-pNPP Assay.[15] ATX activity toward bis-pNPP was determined as follows. In an opaque flat-bottom 384-well plate an amount of 2 μL of DMSO containing inhibitor was added to 24 μL of recombinant ATX (∼40 nM) in Tris-buffered saline (140 mM NaCl, 5 mM KCl, 1 mM CaCl$_2$, 1 mM MgCl$_2$, and 50 mM Tris-HCl, pH 7.8) which contained albumin from bovine serum fatty acid free (BSA-FAF) (0.2 mg mL^{-1}). Finally, 24 μL of bis-pNPP (2 mM) was added to each well and the plate was incubated for 3 h at room temperature. This mixture with DMSO alone was used as a control. For each inhibitor 10 concentrations were measured covering a range of 0.025 to 100 μM to determine IC$_{50}$ values. Percentage inhibition was determined for a final concentration of 5 μM of inhibitor. Absorbance was measured in a Perkin-Elmer Envision plate reader (λ = 405 nm). The absorbance at 0 h was used to correct for molecules that absorb at 405 nm. Data were analyzed using Graphpad Prism software. IC$_{50}$ values and percentage inhibition were determined in three independent experiments for each inhibitor. Percentage of residual activity (RA) is given as bottom value for curve fit.

CPF4 Assay.[15] This assay was carried out in the same manner as the bis-pNPP assay using a substrate concentration of 2 μM. Fluorescence was monitored in a BMG Fluorstar 96-well plate reader (excitation at 355 nm, emission at 460 and 520 nm).

Choline Release Assay.[17] ATX activity using LPC (18:1) as substrate was determined as follows. In an opaque flat-bottom 96-wells plate (Greiner) 1 μL of DMSO containing inhibitor was added to 49 μL of recombinant ATX (∼40 nM) in Tris-HCl buffer (0.01% Triton X-100 and 50 mM Tris-HCl, pH 7.4). Finally, 50 μL of 80 μM LPC (18:1) in Tris-HCl buffer (10 mM MgCl$_2$, 10 mM CaCl$_2$, 0.01% Triton X-100, and 50 mM Tris-HCl, pH 7.4) was added to each well and the plate was incubated at 37 °C. The above-described mixture with DMSO alone was used as a control. LPC without ATX was taken as control for autohydrolysis of LPC. For each inhibitor 10 concentrations were measured covering a range of 0.01 to 30 μM to determine IC$_{50}$ values. Percentage inhibition was determined for a final concentration of 5 μM inhibitor. After 3 h of incubation, 50 μL of ABTS (2 mM) and horseradish peroxidase (5 U mL^{-1}) was added to 50 μL of the reaction mixture and absorbance was measured and used to correct for absorbance of the molecules. Finally, 50 μL of choline oxidase (5 U mL^{-1}) in Tris-HCl (0.01% Triton X-100 and 50 mM Tris-HCl, pH 7.4) was added for colorimetric reaction. Absorbance was measured in a Perkin-Elmer

Envision plate reader (λ = 405 nm). Data were analyzed using Graphpad Prism software.

In addition, the effect of the inhibitors on the enzymatic coloring reaction was investigated using 40 μM choline at 30 μM inhibitor using the above-described coloring reagents. No inhibition of the enzymatic reaction by inhibitors was observed.

Washout of Inhibitors. ATX ($\sim$40 nM) in the same buffer used for the choline release assay was incubated with (5 μM) and without inhibitors at 37 °C. After 20 min the incubation mixtures were washed out with ethyl acetate with 9 times the volume of the ATX solution. The ATX activity of these solutions was determined using the choline release assay.

Chemistry. All chemicals were obtained from Sigma-Aldrich and used without further purification. Dry *N*,*N*-dimethylformamide (DMF) from Biosolve was obtained by treatment with molecular sieves (4 Å). Analytical thin layer chromatography was performed on aluminum sheets precoated with silica gel 60 F$_{254}$. Column chromatography was carried out on silica gel (0.035−0.070, 90 Å, Acros).

For isolation by centrifugation a Heraeus Multifuge 3$_{S-R}$ centrifuge was used. Products were spun at 4400g at 4 °C for 5 min. Nuclear magnetic resonance spectra (^{1}H NMR and COSY) were determined in deuterated dimethyl sulfoxide (DMSO-d_6) using a Bruker ARX 400 spectrometer (^{1}H, 400 MHz) at 298 K, unless indicated otherwise. Peak shapes in the NMR spectra are indicated with the symbols "d" (doublet), "dd" (double doublet), "s" (singlet), "bs" (broad singlet), and "m" (multiplet). Chemical shifts (δ) are given in ppm and coupling constants J in Hz. DMSO (δ = 2.50 ppm) was used as internal reference.

LC−MS measurements were performed on a system equipped with a Waters 2795 separation module (Alliance HT), Waters 2996 photodiode array detector (190−750 nm), Waters Alltima C18 column (2.1 mm × 100 mm), and an LCT orthogonal acceleration time of flight mass spectrometer. Samples were run at a flow rate of 0.40 mL min^{-1} using gradient elution (water/acetonitrile/formic acid) from 950/50/10 (v/v/v) to 50/950/10 (v/v/v). Retention times (t_R) are given in minutes. Purity of all compounds was verified by LC−MS.

The purity of all tested compounds as determined by LC−MS analyses was greater than 95%.

4-[(4-Formyl-2-methoxyphenoxy)methyl]benzoic Acid (7). To a solution of vanillin (1.41 g, 9.24 mmol) and KOH (0.640 g, 11.4 mmol) in DMSO (10 mL), methyl 4-(bromomethyl)-benzoate (2.00 g, 8.73 mmol) was added. The reaction mixture was stirred at room temperature. After 30 min, water (50 mL) was added. The solution was heated at 393 K for 2 h. Subsequently, 1 M NaOH (aq) (10 mL) was added under reflux until the solution became clear. Finally, the reaction mixture was poured into water and was acidified with 1 M HCl to pH 2. The precipitate was isolated by centrifugation, washed with water, and lyophilized resulting in the title compound.
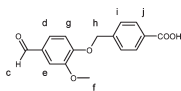
Yield: 91%. ^{1}H NMR: δ = 12.99 (bs, 1H, OH), 9.85 (s, 1H, c), 7.98 (d, *J* 8.3, 2H, j), 7.58 (d, *J* 8.3, 2H, i), 7.55 (dd, *J* 1.9 and 8.3, 1H, d), 7.44 (d, *J* 1.8, 1H, e), 7.26 (d, *J* 8.3, 1H, g), 5.32 (s, 2H, h), 3.86 (s, 3H, f). MS: *m/z* [M + H]$^+$ calcd 287.09, obsd 287.11. LC: t_R = 7.75.

Synthesis of 3-(4-Fluorobenzyl)-1,3-thiazolane-2,4-dione (8). To a cooled solution (0 °C) of thiazolidine-2,4-dione (5.87 g, 50 mmol) in DMF (100 mL), sodium hydride (60% in oil, 1.8 g, 45 mmol) was added. A solution of 1-(chloromethyl)-4-fluor-obenzene (4.3 mL, 36.8 mmol) in DMF (25 mL) was added to the reaction mixture. The mixture was allowed to warm to room

temperature and was stirred for 4 h. Then the mixture was poured into ice−water (250 mL), and hexane (100 mL) was added. After a night at 4 °C the precipitated crystals were filtered and dried to give a white solid.
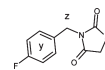
Yield: 74%. ^{1}H NMR: δ = 7.34−7.14 (m, 4H, y), 4.65 (s, 2H, z), 4.26 (s, 2H, b). MS: *m/z* [M + H]$^+$ calcd 226.03, obsd 226.04. LC: t_R = 8.22.

General Method for the Synthesis of (2,4-Dioxo-1,3-thiazolan-5-yliden)benzoic Acids and Benzeneboronic Acids. To a solution of 1,3-thiazolane-2,4-dione **8** (0.293 mmol) in ethanol (2.5 mL), piperidine (12 μL, 0.207 mmol) and the appropriate aldehyde (0.352 mmol) were added, and the solution was refluxed for 22 h. When the mixture was cooled to room temperature, the product precipitated out of solution. Centrifugation and washing with ethanol gave a homogeneous compound.

4-[(4-{[3-(4-Fluorobenzyl)-2,4-dioxo-1,3-thiazolan-5-yliden]-methyl}-2-methoxyphenoxy)methyl]benzoic Acid (2).
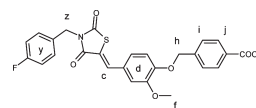

Yield: 63%. COSY was used to assign chemical shifts. ^{1}H NMR: δ = 12.99 (bs, 1H, OH), 7.97 (d, *J* 8.3, 2H, j), 7.92 (s, 1H, c), 7.56 (d, *J* 8.3, 2H, i), 7.38−7.16 (m, 7H, d + g + y), 5.27 (s, 2H, h), 4.82 (s, 2H, z), 3.84 (s, 3H, f). MS: *m/z* [M − H]$^-$ calcd 492.10, obsd 492.10. LC: t_R = 10.54.

3-[(4-{[3-(4-Fluorobenzyl)-2,4-dioxo-1,3-thiazolan-5-yliden]-methyl}phenoxy)methyl]benzeneboronic Acid (72).
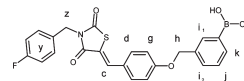

Yield: 64%. ^{1}H NMR: δ = 8.08 (s, 2H, OH), 7.92 (s, 1H, c), 7.87 (s, 1H, i$_2$), 7.76 (d, *J* 7.4, 1H, i$_1$), 7.60 (d, *J* 7.1, 2H, d), 7.50−7.16 (m, 10H, d + g + k + j + x + y), 5.18 (s, 2H, h), 4.82 (s, 2H, z). MS: *m/z* [M +H]$^+$ calcd 464.11, obsd 464.25. LC: t_R = 10.77.

4-[(4-{[3-(4-Fluorobenzyl)-2,4-dioxo-1,3-thiazolan-5-yliden]-methyl}phenoxy)methyl]benzeneboronic Acid (73).
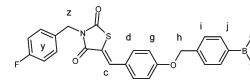

Yield: 81%. ^{1}H NMR: δ = 8.05 (s, 2H, OH), 7.93 (s, 1H, c), 7.81 (d, *J* 8.0, 2H, j), 7.61 (d, *J* 8.9, 2H, d), 7.42 (d, *J* 8.3, 2H, i), 7.41−7.16 (m, 6H, g + y), 5.21 (s, 2H, h), 4.82 (s, 2H, z). MS: *m/z* [M + H]$^+$ calcd 464.11, obsd 464.21. LC: t_R = 10.45.

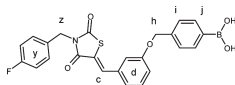**2-[(4-{[3-(4-Fluorobenzyl)-2,4-dioxo-1,3-thiazolan-5-yliden]-methyl}phenoxy)methyl]benzeneboronic Acid (74).**
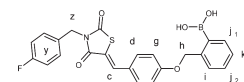
Yield: 48%. ^{1}H NMR: δ = 8.10 (s, 2H, OH), 7.93 (s, 1H, c), 7.62−7.13 (m, 12H, d + g + i + j$_{1+2}$ + k + y), 5.32 (s, 2H, h), 4.82 (s, 2H, z). MS: *m/z* [M + H]$^+$ calcd 464.11, obsd 464.12. LC: t_R = 10.67.

3-[(3-{[3-(4-Fluorobenzyl)-2,4-dioxo-1,3-thiazolan-5-yliden]-methyl}phenoxy)methyl]benzeneboronic Acid (75).
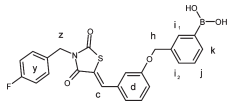
Yield: 40%. ^{1}H NMR: δ = 8.10 (bs, 2H, OH), 7.94 (s, 1H, c), 7.87 (s, 1H, i$_2$), 7.76 (d, J 7.3, 1H, k), 7.51–7.16 (m, 10H, d + i$_1$ + j + y), 5.16 (s, 2H, h), 4.82 (s, 2H, z). MS: m/z [M + H]$^+$ calcd 464.11, obsd 464.13. LC: t_R = 10.72.

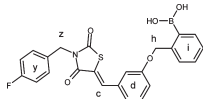**4-[(3-{[3-(4-Fluorobenzyl)-2,4-dioxo-1,3-thiazolan-5-yliden]-methyl}phenoxy)methyl]benzeneboronic Acid (76).**

Yield: 26%. ^{1}H NMR: δ = 8.07 (s, 2H, OH), 7.93 (s, 1H, c), 7.81 (d, J 8.0, 2H, j), 7.49–7.16 (m, 10H, d + i + y), 5.19 (s, 2H, h), 4.82 (s, 2H, z). MS: m/z [M + H]$^+$ calcd 464.11, obsd 464.12. LC: t_R = 10.70.

2-[(3-{[3-(4-Fluorobenzyl)-2,4-dioxo-1,3-thiazolan-5-yliden]-methyl}phenoxy)methyl]benzeneboronic Acid (77).

Yield: 32%. ^{1}H NMR: δ = 8.09 (s, 2H, OH), 7.94 (s, 1H, c), 7.57–7.12 (m, 12H, d + i + y), 5.29 (s, 2H, h), 4.83 (s, 2H, z). MS: m/z [M + H]$^+$ calcd 464.11, obsd 464.13. LC: t_R = 10.73.

Supporting Information Available: Information about the screening of an NCI collection and the synthetic procedures and analytical data for compounds **9**−**30**. This material is available free of charge via the Internet at http://pubs.acs.org.

References

(1) Gijsbers, R.; Aoki, J.; Arai, H.; Bollen, M. The hydrolysis of lysophospholipids and nucleotides by autotaxin (NPP2) involves a single catalytic site. *FEBS Lett.* **2003**, *538*, 60–64.
(2) Clair, T.; Lee, H. Y.; Liotta, L. A.; Stracke, M. L. Autotaxin is an exoenzyme possessing 5'-nucleotide phosphodiesterase/ATP pyrophosphatase and ATPase activities. *J. Biol. Chem.* **1997**, *272*, 996–1001.
(3) Bollen, M.; Gijsbers, R.; Ceulemans, H.; Stalmans, W.; Stefan, C. Nucleotide pyrophosphatases/phosphodiesterases on the move. *Crit. Rev. Biochem. Mol. Biol.* **2000**, *35*, 393–432.
(4) Tokumura, A.; Majima, E.; Kariya, Y.; Tominaga, K.; Kogure, K.; Yasuda, K.; Fukuzawa, K. Identification of human plasma lysophospholipase D, a lysophosphatidic acid-producing enzyme, as autotaxin, a multifunctional phosphodiesterase. *J. Biol. Chem.* **2002**, *277*, 39436–39442.
(5) Umezu-Goto, M.; Kishi, Y.; Taira, A.; Hama, K.; Dohmae, N.; Takio, K.; Yamori, T.; Mills, G. B.; Inoue, K.; Aoki, J.; Arai, H. Autotaxin has lysophospholipase D activity leading to tumor cell growth and motility by lysophosphatidic acid production. *J. Cell Biol.* **2002**, *158*, 227–233.
(6) Moolenaar, W. H.; van Meeteren, L. A.; Giepmans, B. N. The ins and outs of lysophosphatidic acid signaling. *BioEssays* **2004**, *26*, 870–881.
(7) van Meeteren, L. A.; Ruurs, P.; Stortelers, C.; Bouwman, P.; van Rooijen, M. A.; Pradere, J. P.; Pettit, T. R.; Wakelam, M. J.; Saulnier-Blache, J. S.; Mummery, C. L.; Moolenaar, W. H.; Jonkers, J. Autotaxin, a secreted lysophospholipase D, is essential for blood vessel formation during development. *Mol. Cell. Biol.* **2006**, *26*, 5015–5022.
(8) Tanaka, M.; Okudaira, S.; Kishi, Y.; Ohkawa, R.; Iseki, S.; Ota, M.; Noji, S.; Yatomi, Y.; Aoki, J.; Arai, H. Autotaxin stabilizes blood vessels and is required for embryonic vasculature by producing lysophosphatidic acid. *J. Biol. Chem.* **2006**, *281*, 25822–25830.
(9) van Meeteren, L.; Moolenaar, W. Regulation and biological activities of the autotaxin−LPA axis. *Prog. Lipid Res.* **2007**, *46*, 145–160.
(10) David, M.; Wannecq, E.; Descotes, F.; Jansen, S.; Deux, B.; Ribeiro, J.; Serre, C. M.; Gres, S.; Bendriss-Vermare, N.; Bollen, M.; Saez, S.; Aoki, J.; Saulnier-Blache, J. S.; Clezardin, P.; Peyruchaud, O. Cancer cell expression of autotaxin controls bone metastasis formation in mouse through lysophosphatidic acid-dependent activation of osteoclasts. *PLoS One* **2010**, *5*, e9741.
(11) Kanda, H.; Newton, R.; Klein, R.; Morita, Y.; Gunn, M.; Rosen, S. Autotaxin, an ectoenzyme that produces lysophosphatidic acid, promotes the entry of lymphocytes into secondary lymphoid organs. *Nat. Immunol.* **2008**, *9*, 415–423.
(12) Tager, A.; LaCamera, P.; Shea, B.; Campanella, G.; Selman, M.; Zhao, Z.; Polosukhin, V.; Wain, J.; Karimi-Shah, B.; Kim, N.; Hart, W.; Pardo, A.; Blackwell, T.; Xu, Y.; Chun, J.; Luster, A. The lysophosphatidic acid receptor LPA1 links pulmonary fibrosis to lung injury by mediating fibroblast recruitment and vascular leak. *Nat. Med.* **2008**, *14*, 45–54.
(13) Meyer zu Heringdorf, D.; Jakobs, K. H. Lysophospholipid receptors: signalling, pharmacology and regulation by lysophospholipid metabolism. *Biochim. Biophys. Acta* **2007**, *1768*, 923–940.
(14) Murakami, M.; Shiraishi, A.; Tabata, K.; Fujita, N. Identification of the orphan GPCR, P2Y10 receptor as the sphingosine-1-phosphate and lysophosphatidic acid receptor. *Biochem. Biophys. Res. Commun.* **2008**, *371*, 707–712.
(15) van Meeteren, L. A.; Ruurs, P.; Christodoulou, E.; Goding, J. W.; Takakusa, H.; Kikuchi, K.; Perrakis, A.; Nagano, T.; Moolenaar, W. H. Inhibition of autotaxin by lysophosphatidic acid and sphingosine 1-phosphate. *J. Biol. Chem.* **2005**, *280*, 21155–21161.
(16) Gajewiak, J.; Tsukahara, R.; Fujiwara, Y.; Tigyi, G.; Prestwich, G. D. Synthesis, pharmacology, and cell biology of sn-2-aminooxy analogues of lysophosphatidic acid. *Org. Lett.* **2008**, *10*, 1111–1114.
(17) Cui, P.; Tomsig, J.; McCalmont, W.; Lee, S.; Becker, C.; Lynch, K.; Macdonald, T. Synthesis and biological evaluation of phosphonate derivatives as autotaxin (ATX) inhibitors. *Bioorg. Med. Chem. Lett.* **2007**, *17*, 1634–1640.
(18) Guowei, J.; Yong, X.; Yuko, F.; Tamotsu, T.; Ryoko, T.; Joanna, G.; Gabor, T.; Prestwich, G. D. Alpha-substituted phosphonate analogues of lysophosphatidic acid (LPA) selectively inhibit production and action of LPA. *ChemMedChem* **2007**, *2*, 679–690.
(19) Ferry, G.; Moulharat, N.; Pradere, J.; Desos, P.; Try, A.; Genton, A.; Giganti, A.; Beucher-Gaudin, M.; Lonchampt, M.; Bertrand, M.; Saulnier-Blache, J.; Tucker, G.; Cordi, A.; Boutin, J. S32826, a nanomolar inhibitor of autotaxin: discovery, synthesis and applications as a pharmacological tool. *J. Pharmacol. Exp. Ther.* **2008**, *327*, 809–819.
(20) van Meeteren, L.; Brinkmann, V.; Saulnier-Blache, J.; Lynch, K.; Moolenaar, W. Anticancer activity of FTY720: phosphorylated FTY720 inhibits autotaxin, a metastasis-enhancing and angiogenic lysophospholipase D. *Cancer Lett.* **2008**, *266*, 203–208.
(21) Moulharat, N.; Fould, B.; Giganti, A.; Boutin, J.; Ferry, G. Molecular pharmacology of adipocyte-secreted autotaxin. *Chem.-Biol. Interact.* **2008**, *172*, 115–124.
(22) Parrill, A.; Echols, U.; Nguyen, T.; Pham, T.; Hoeglund, A.; Baker, D. Virtual screening approaches for the identification of non-lipid autotaxin inhibitors. *Bioorg. Med. Chem.* **2008**, *16*, 1784–1795.
(23) Hoeglund, A.; Bostic, H.; Howard, A.; Wanjala, I.; Best, M.; Baker, D.; Parrill, A. Optimization of a pipemidic acid autotaxin inhibitor. *J. Med. Chem.* **2009**, *53*, 1056–1066.
(24) Albers, H. M.; Dong, A.; van Meeteren, L. A.; Egan, D. A.; Sunkara, M.; van Tilburg, E. W.; Schuurman, K.; van Tellingen, O.; Morris, A. J.; Smyth, S. S.; Moolenaar, W. H.; Ovaa, H. Boronic acid-based inhibitor of autotaxin reveals rapid turnover of LPA in the circulation. *Proc. Natl. Acad. Sci. U.S.A.* **2010**, *107*, 7257–7262.
(25) Takakusa, H.; Kikuchi, K.; Urano, Y.; Sakamoto, S.; Yamaguchi, K.; Nagano, T. Design and synthesis of an enzyme-cleavable sensor molecule for phosphodiesterase activity based on fluorescence resonance energy transfer. *J. Am. Chem. Soc.* **2002**, *124*, 1653–1657.
(26) Saunders, L. P.; Ouellette, A.; Bandle, R.; Chang, W. C.; Zhou, H.; Misra, R. N.; De La Cruz, E. M.; Braddock, D. T. Identification of

small-molecule inhibitors of autotaxin that inhibit melanoma cell migration and invasion. *Mol. Cancer Ther.* **2008**, *7*, 3352–3362.

(27) Johnstone, R.; Rose, M. A rapid, simple, and mild procedure for alkylation of phenols, alcohols, amides and acids. *Tetrahedron* **1979**, *35*, 2169–2173.

(28) Bruno, G.; Costantino, L.; Curinga, C.; Maccari, R.; Monforte, F.; Nicolo, F.; Ottana, R.; Vigorita, M. G. Synthesis and aldose reductase inhibitory activity of 5-arylidene-2,4-thiazolidinediones. *Bioorg. Med. Chem.* **2002**, *10*, 1077–1084.

(29) Groll, M.; Berkers, C.; Ploegh, H.; Ovaa, H. Crystal structure of the boronic acid-based proteasome inhibitor bortezomib in complex with the yeast 20S proteasome. *Structure* **2006**, *14*, 451–456.

(30) Crompton, I. E.; Cuthbert, B. K.; Lowe, G.; Waley, S. G. Beta-lactamase inhibitors. The inhibition of serine beta-lactamases by specific boronic acids. *Biochem. J.* **1988**, *251*, 453–459.

(31) Kuivila, H.; Armour, A. Electrophilic displacement reactions. IX. Effects of substituents on rates of reactions between hydrogen peroxide and benzeneboronic acid. *J. Am. Chem. Soc.* **1957**, *79*, 5659–5662.

(32) Kuivila, H. Electrophilic displacement reactions. VI. Catalysis by strong acids in the reaction between hydrogen peroxide and benzeneboronic acid. *J. Am. Chem. Soc.* **1955**, *77*, 4014–4016.

(33) Snyder, H. R.; Kuck, J. A.; Johnson, J. Organoboron compounds, and the study of reaction mechanisms. Primary aliphatic boronic acids. *J. Am. Chem. Soc.* **1938**, *60*, 105–111.